Computer Modeling in Engineering & Sciences

Tech Science Press

DOI: 10.32604/cmes.2024.046740

ARTICLE

Research on Cavitation Characteristics and Influencing Factors of Herringbone Gear Pump

Jinlong Yang, Kwang-Hee Lee and Chul-Hee Lee*

Department of Mechanical Engineering of Inha University, Incheon, 22212, South Korea

*Corresponding Author: Chul-Hee Lee. Email: chulhee@inha.ac.kr

Received: 13 October 2023 Accepted: 29 December 2023 Published: 11 March 2024

ABSTRACT

Cavitation is a common issue in pumps, causing a decrease in pump head, a fall in volumetric efficiency, and an intensification of outlet flow pulsation. It is one of the main hazards that affect the regular operation of the pump. Research on pump cavitation mainly focuses on mixed flow pumps, jet pumps, external spur gear pumps, etc. However, there are few cavitation studies on external herringbone gear pumps. In addition, pumps with different working principles significantly differ in the flow and complexity of the internal flow field. Therefore, it is urgent to study the cavitation characteristics of external herringbone gear pumps. Compared with experimental methods, visual research and cavitation area identification are achieved through computation fluid dynamic (CFD), and changing the boundary conditions and shape of the gear rotor is easier. The simulation yields a head error of only 0.003% under different grid numbers, and the deviation between experimental and simulation results is less than 5%. The study revealed that cavitation causes flow pulsation at the outlet, and the cavitation serious area is mainly distributed in the meshing gap and meshing area. Cavitation can be inhibited by reducing the speed, increasing the inlet pressure, and changing the helix angle can be achieved. For example, when the inlet pressure is 5 bar, the maximum gas volume fraction in the meshing area is less than 50%. These results provide a reference for optimizing the design and finding the optimal design parameters to reduce or eliminate cavitation.

KEYWORDS

Herringbone gear pump; cavitation; rotating speed; inlet pressure; helix angle; TwinMesh

Nomenclature

CFD	Computational fluid dynamics
N–S	Navier–Stokes
RNG	Renormalization Group
SST	Shear–Stress Transport

e.g.

$\varnothing$	Porosity
s	Skin factor
p_x	Fluid pressure

p_v	The saturated vapor pressure of a liquid at a given temperature
ρ	Density of a liquid
v_∞	Flow rate of a fluid
σ	Cavitation number
κ	Turbulent kinetic energy
ε	Dissipation rate
μ_t	Turbulent viscosity
G_k	Average velocity turbulent kinetic energy
G_b	Buoyancy turbulent kinetic energy
Y_M	Total dissipation rate
S_K	User-defined conditions (Term generated by turbulent kinetic energy)
S_ε	User-defined conditions (Term generated by turbulent dissipation)
ρ_v	The density of the vapor
ρ_l	Density of the liquid
f	Steam mass fraction
α	Steam volume fraction
R_e	Steam generation rate
R_c	Steam condensation rate
R_B	The radius of the bubble
p_B	The internal pressure of the drum
p	Pressure around the bubble in the liquid
R	Net phase transition rate
n	Number of vacuoles
V_{ch}	Characteristic velocity
C_e (C_c)	Empirical coefficients
$\sqrt{k}$	The square root of the local turbulent kinetic energy
β	Gear helix angle

1 Introduction

Cavitation in hydraulic systems occurs when air separates from the gas in a region where the fluid's partial pressure is lower than the air separation pressure [1]. This results in the occurrence of gas-liquid two-phase flow [2,3]. Cavitation is one of the most challenging fluid flow anomalies affecting the flow behavior and physical characteristics of pumps [4,5]. During the operation of the system, the formation and collapse of vapor bubbles in the liquid due to low-pressure conditions [6] disrupt the smooth flow of fluid [7] and reduce the ability of the liquid to provide the required flow and pressure [8], decreasing the pump efficiency [9] and performance [10]. Simultaneous rupture produces shock waves that cause pitting, erosion, and wear, resulting in vibration and noise [11]. Experimental methods have been conducted to examine pump cavitation [12,13], allowing direct measurement and collection of data on essential parameters, such as pressure fluctuations, noise levels, vibrations, and flow patterns. On the other hand, cavitation usually occurs inside the impeller or in areas that are not easily observed directly. Moreover, the internal flow is difficult to visualize, limiting understanding of the internal flow behavior. These defects have placed some obstacles to the research on the cavitation mechanism and the optimization of pump structure and materials. With the improvement of computer performance, computational fluid dynamics (CFD) analysis allows an in-depth study of the pump cavitation phenomenon [14,15]. Initially, detailed and comprehensive data can be provided, allowing the visualization and analysis of internal flow phenomena, enhancing the understanding of cavitation

mechanisms, and helping identify potential problems. Second, parameter sensitivity can be performed, systematically varying the different parameters and evaluating their impact on cavitation. Finally, the parameters and boundary conditions within the virtual model can be modified easily, enabling the rapid iteration and exploration of different design options helping optimize the design of hydraulic systems to minimize or eliminate the effects of cavitation. Therefore, CFD analysis can provide an effective tool for studying the mechanism and impact of cavitation, particularly for the visualization of internal flow conditions. The inside of the pump involves complex flow and hydraulic characteristics, and liquid flow simulation requires a finer mesh quality. A high-resolution grid is necessary to describe the flow field boundary layer flow and interstitial flow to reduce oscillation or numerical dissipation and improve the simulation quality. On the other hand, a high-quality hexahedral grid is required to represent the complex geometries accurately, avoid shape distortion and node irregularities caused by tetrahedral grids, and describe the direction and gradient of flow more accurately, which is particularly important for simulations involving complex flow phenomena, such as turbulence. To ensure simulation accuracy, a volumetric rotating machinery meshing tool developed by CFX-Berlin–TwinMesh can be utilized. This tool can automatically generate high-quality hexahedral meshes. Users can define mesh parameter properties such as the number of meshes, height of the first layer grid, and change ratio. Advanced front-back smoothing technology can be employed to achieve a smaller internal angle (perpendicular to the wall) and volume change ratio. By integrating with the CFX solver, a comprehensive solution can be obtained [16]. The automation level of simulation and the simulation quality can be improved as a result [17]. Therefore, this study uses an analysis method combining TwinMesh with CFX.

The current leading research uses CFD to simulate the process of forming bubbles and air pockets and to predict the possibility of cavitation and the impact of cavitation. Regarding pump cavitation research, scholars have studied the cavitation generation mechanisms and effects of different types of pumps. For mixed-flow pumps, Li et al. [18] found that cavitation reduces the output power of the impeller, resulting in a decrease in head and unstable operation. For external gear pumps, Del Campo et al. [19] used a simplified two-dimensional numerical method to conduct simulations to study the impact of cavitation on volumetric efficiency. Fu et al. [20] studied the cavitation characteristics under steady and transient cavitation conditions for centrifugal pumps. When cavitation is severe, cavitation affects the impeller radial force and impeller channel—the flow pattern within the flow pattern. Wang et al. [21] studied the characteristics of irreversible energy loss caused by cavitation flow in centrifugal pumps by the entropy production theory with CFD. For jet pumps, Cunningham et al. [22] studied the reasons for cavitation in jet pumps, resulting in decreased efficiency. In addition, Ouyang et al. [23] studied cavitation caused by vibration during high-speed gear transmission, considering the gear cavitation mechanism of pitting corrosion and cracks. These studies mainly focus on the generation mechanism of cavitation and the impact of cavitation on efficiency, head, energy loss, and flow, providing a reference for the design of different types of pumps.

This study examines the effects of cavitation on the pump operation process and simulates the internal flow through the visualization tool (CFD). The simulation results are verified experimentally. On the other hand, the research results have limited effects on the optimal design of certain types of pumps because most studies only study the influence of one or several factors. The influence of fluid characteristics [24–26], boundary conditions [27,28], and internal structure [29,30] on cavitation should be comprehensively considered. Regarding fluid characteristics, for example, high-viscosity liquids make it difficult and dangerous to expel air bubbles. For boundary conditions, for example, a low inlet pressure will cause the liquid pressure to reach below the gas saturation vapor pressure, quickly generating bubbles. The internal structure, such as the shape of the rotor, directly affects the

liquid's flow and pressure distribution, which will significantly impact cavitation. Pumps with different working principles differ significantly in the flow and complexity of the internal flow field [31]. The fluid chamber for suction and discharge produces positive meshing and side gushing, while the spur gear pump realizes the suction and discharge of fluid in the pump chamber through the meshing of spur gears. During the meshing process of the herringbone gear, cavities of different sizes are formed when moving from the root to the tip. Consequently, cavitation characteristics vary depending on the type of pump. External meshing herringbone gear pumps exhibit robust resistance to high working pressures, adapt well to high-viscosity fluids, possess self-priming capabilities, and are easily maintainable, making them indispensable in production processes. However, limited research has been conducted on cavitation in external meshing herringbone gear pumps. Given this context, it becomes imperative to conduct a dedicated study on the cavitation characteristics of external herringbone gear pumps.

Therefore, this study takes the external meshing herringbone gear pump as the research object and studies the cavitation mechanism of the external meshing herringbone gear pump at high speed and the method to reduce the occurrence of cavitation by CFD. The reason is that the CFD method provides a visualization tool that is difficult to achieve through experiments, which helps understand the mechanism of cavitation and identify the area where cavitation occurs. Compared with the experimental method, it is easier to change the boundary conditions, which is beneficial to studying the external meshing herringbone gear pump. Explore the suitable operating conditions of the pump; the parameters of the gear rotor are easy to change, shortening development time and reducing development costs. The advantage of the study lies in the choice of the TwinMesh + CFX tool to obtain a more accurate solution based on the current simulation problems and the principle of cavitation, focusing on the transient changes in the gas volume fraction and pressure in the meshing area during the meshing process to observe the influence of cavitation more directly. Unlike other types of pumps, this study also selects helix angle as the main influencing factor in addition to exploring conditions such as speed and inlet pressure. The helix angle significantly affects the meshing and disengagement of the gear during rotation, thus affecting the pressure distribution in the pump; the flow pattern is affected by the smoothness of the meshing, and a suitable helix angle can ensure continuous and even flow of liquid due to the influence of pressure changes along the gear teeth. Therefore, an inappropriate helix angle will lead to uneven pressure distribution and quickly form vapor bubbles in the liquid, leading to cavitation and other occurrences. This supplements the research on cavitation characteristics of external meshing herringbone gear pumps. Targeted research on external meshing herringbone gear pumps can help reduce or eliminate the effects of cavitation.

2 Cavitation

Cavitation significantly impacts the flow of liquids and the performance of fluid equipment [32], mainly when it occurs at high speed and high pressure. Liquids are usually mixed with a certain proportion of gas. For example, the air content in water is approximately 1.87% at standard atmospheric pressure and temperature. When the pressure is lower than the cavitation separation pressure, the air dissolved in the liquid will separate from the liquid and gather into bubbles to dissociate in the liquid. This phenomenon is called gas cavitation. The liquid will vaporize to produce many steam bubbles when the pressure is lower than the saturated vapor pressure, resulting in severe steam cavitation [33]. The precipitated gas exists in the liquid in the form of voids and moves forward with the flow of the liquid. The volume of the cavity increases continuously as the pressure of the fluid continues to decrease. On the other hand, the external pressure is higher than the pressure inside the pit when the cavity moves to a place with higher pressure, and the hole volume will continue to shrink

until it is crushed. The strong impact force, high temperature, and high-speed jet generated during the crushing process will damage the surface of various parts, contaminate the liquid, and affect the performance parameters of the pump, such as the head, flow rate, and efficiency [34].

2.1 Cavitation Number

The cavitation number is an important parameter that describes whether cavitation occurs in a liquid, and it is defined as [35]:

$$\sigma = \frac{p_x - p_v}{\frac{1}{2}\rho v_\infty^2} \tag{1}$$

where p_x is the fluid pressure; p_v is the saturated vapor pressure of a liquid at a given temperature; ρ is the density of a liquid; v_∞ is the flow rate of a fluid.

The size of the σ value represents different cavitation states; a smaller σ value means easier cavitation generation. Therefore, a smaller $(p_x - p_v)$ value, i.e., a smaller difference between the pressure of the fluid and the saturated vapor pressure of the liquid, indicates a smaller σ value and easier cavitation. A smaller v_∞ value means a larger σ value. Hence, cavitation is difficult. In addition, a greater liquid density ρ means a smaller σ value, making cavitation easier. Combined with the fluid motion equation, the factors affecting cavitation can include geometry, liquid, liquid temperature, and flow velocity.

2.2 Basic Equations of Cavitation Numerical Simulation

The key to a mathematical solution to cavitation phenomena is to establish a suitable cavitation model that can simultaneously describe the characteristics of cavitation at two different time scales and the mass exchange between gas–liquid two-phase flow [36]. The free-stream-line theory and the Hodograph method are first proposed as a mathematical solution to cavitation phenomena. On this basis, cavitation theoretical calculation methods, such as mapping and reflux models, are derived. These methods are attributed to fluid simplification (incompressible and no viscosity, assuming that the internal pressure of the cavity is constant, and the surface of the hole is a free streamline). Therefore, studying the development and collapse process of a bubble is challenging. The shortcomings of the above-mentioned potential flow theory models are overcome using a cavitation model based on the N–S (Navier–Stokes) equation, which fully considers the influence of fluid viscosity on the formation, development, and collapse of cavitation. This model is combined with the turbulence model to analyze unsteady cavitation. On the other hand, there are certain limitations in studying fluid viscosity, turbulent flow, and fluid compressibility. The influence of the two-phase flow phase change rate, bubble dynamics, and turbulent fluctuations on cavitation is considered using the gas phase mass fraction transport equation based on the Full cavitation model of the two-phase flow idea. The cavitation numerical simulation method based on the N–S equation is relatively mature and used widely. Therefore, follow-up studies will use this method as the theoretical basis for research.

2.2.1 Turbulence Model

CFD is based on classical fluid mechanics and numerical analysis and mainly on three significant equations (continuity equation, momentum conservation equation, and energy conservation equation) to solve and analyze fluid motion.

In cavitation research, the turbulence model predicts the complex gas–liquid flow in the external meshing herringbone gear pump [37]. Commonly used turbulence models include the standard

κ–ε model, the Renormalization Group (RNG) κ–ε model, κ–w model group, and the Shear–Stress Transport (SST) κ–w model. The choice of turbulence model affects the accuracy and reliability of the simulation results, affecting pump design and optimization.

The standard κ–ε model transport equation is a semi-empirical model based on the model transport equation of turbulent kinetic energy κ and its dissipation rate ε. Eqs. (2) and (3) present its transport equation [38]:

$$\frac{\partial}{\partial t}(\rho\kappa)+\frac{\partial}{\partial x_i}(\rho\kappa\mu_i)=\frac{\partial}{\partial x_j}\left[\left(\mu+\frac{\mu_t}{\sigma_k}\right)\frac{\partial\kappa}{\partial x_j}+G_k+G_b-\rho\varepsilon-Y_M+S_k\right. \tag{2}$$

$$\frac{\partial}{\partial t}(\rho\varepsilon)+\frac{\partial}{\partial x_i}(\rho\varepsilon\mu_i)=\frac{\partial}{\partial x_j}\left[\left(\mu+\frac{\mu_t}{\sigma_\varepsilon}\right)\frac{\partial\varepsilon}{\partial x_i}\right]+G_{1\varepsilon\frac{\varepsilon}{\kappa}}(G_k+G_{3\varepsilon}G_b)-C_{2\varepsilon}\rho\frac{\varepsilon^2}{\kappa}+S_\varepsilon \tag{3}$$

The turbulent viscosity μ_t [39] is proportional to the ratio of the second power of the turbulent kinetic energy κ^2 to the rough dissipation rate ε (the relationship is shown in Eq. (4)):

$$\mu_t=\rho C_\mu\frac{\kappa^2}{\varepsilon} \tag{4}$$

where G_k is the average velocity turbulent kinetic energy; G_b is the buoyancy turbulent kinetic energy; Y_M is the total dissipation rate; S_K and S_ε are user-defined conditions.

The standard κ–ε model has a simple structure and good convergence [40] and is used widely in fluid calculations. Nevertheless, the standard κ–ε model has defects in cavitation simulation. The standard κ–ε model is not designed explicitly to account for phase transition phenomena, such as vaporization and condensation, which are at the heart of cavitation. The standard κ–ε model assumes the flow is incompressible, but cavitation causes pressure changes and phase transitions, producing a compressibility effect. Therefore, the standard κ–ε model is unsuitable for cavitation simulation.

Based on the standard κ–ε model, the RNG κ–ε model adds an R term to the turbulence dissipation rate ε equation. The vortex phenomenon in the turbulence makes the turbulence simulation more accurate. The mathematical expression is as follows:

$$\frac{\partial}{\partial t}(\rho\varepsilon)+\frac{\partial}{\partial x_i}(\rho\varepsilon\mu_i)=\frac{\partial}{\partial x_j}\left[\left(\mu+\frac{\mu_t}{\sigma_\varepsilon}\right)\frac{\partial\varepsilon}{\partial x_i}\right]+G_{1\varepsilon\frac{\varepsilon}{\kappa}}(G_k+G_{3\varepsilon}G_b)-C_{2\varepsilon}\rho\frac{\varepsilon^2}{\kappa}+S_\varepsilon-R_\varepsilon \tag{5}$$

The RNG κ–ε model solves some limitations and defects of the standard κ–ε model [41] and can provide more accurate predictions in complex flows (adverse pressure gradients, swirling flows, and separation), enhanced near-wall processing, improved prediction of wall boundary flow. The model has swirling solid flow and high shear rate advantages, making it more suitable for complex cavitation simulation calculations [41–43].

In addition, the κ–ω turbulence model uses the pulsation frequency ω (Turbulent Frequency) to replace the ε equation in the standard κ–ε model. The turbulent kinetic energy (κ) equation is the same as Eq. (2), and the specific rough dissipation rate (ω) equation is as follows:

$$\frac{\partial}{\partial t}(\rho\omega)+\frac{\partial}{\partial x_i}(\rho\omega\mu_i)=\frac{\partial}{\partial x_j}\left[\left(\mu+\frac{\mu_t}{\sigma_\omega}\right)\frac{\partial\omega}{\partial x_i}\right]+G_{1\omega\frac{\omega}{\kappa}}(G_k+G_{3\omega}G_b)-C_{2\omega}\rho\frac{\omega^2}{\kappa}+S_\omega \tag{6}$$

On the other hand, the κ–ω turbulence model is challenging when dealing with complex flows with severe eddies and significant separations. At the same time, the simulation accuracy is also affected by

the choice of turbulence model constants and grid quality [44]. Therefore, simulations that rely on simulator experience are unsuitable for this study.

The SST κ–ω turbulence model [45,46] combines the κ–ω turbulence model in the inner layer of the boundary layer, with the standard κ–ε model in the shear layer and boundary edge. This combination allows for a unique flow field treatment method and provides certain advantages in simulating back pressure gradient or separation flow. However, it generates significant turbulence and is not suitable for accurately analyzing unsteady dynamic phenomena of cavitation. In contrast, the RNG κ–ε turbulence model is better suited for simulating cavitation in the external meshing herringbone gear pump.

2.2.2 Cavitation Model

The cavitation model is mainly a mathematical model proposed based on fluid mechanics, cavitation dynamics, and other knowledge. The cavitation model based on the potential flow theory does not consider the viscosity of the liquid and is only suitable for the study of some particular cavitation problems. The model cannot accurately solve the cavitation problem in the hydraulic system; the cavitation model is based on the N–S equation. On the other hand, there are some difficulties in studying turbulent flow and fluid compressibility, particularly in solving three-dimensional void flow problems. Singhal et al. proposed the Full cavitation model based on two-phase flow. This model established the transport equation of the vapor phase volume fraction, considering the phase transition rate of the two-phase flow, cavitation dynamics, and turbulent fluctuations [47]. The Full cavitation model is used widely in cavitation simulations because it can provide more accurate predictions of cavitation behavior and is suitable for more complex cavitation flow calculations.

The Full cavitation model uses the Rayleigh–Plesset equation to solve the dynamic process of bubble changes [48,49] and comprehensively considers the influence of liquid compressibility, non-condensable gas, and vapor evaporation and condensation on the simulation results. The following derivation process refers to the Full cavitation model that Singhal et al. proposed based on a two-phase flow [47].

The density of the fluid in this model is related to the vapor mass fraction i as follows:

$$\frac{1}{\rho} = \frac{f}{\rho_v} + \frac{1-f}{\rho_l} \tag{7}$$

where ρ is the density of the mixed liquid, ρ_v is the density of the vapor, and ρ_l is the density of the liquid.

The relationship between steam volume fraction α and steam mass fraction f is as follows:

$$\alpha = f\frac{\rho}{\rho_v} \tag{8}$$

f is determined by the transport equation:

$$\frac{\partial}{\partial t}(\rho f) + \nabla \cdot \left(\rho \vec{V} f\right) = \nabla \cdot (\Gamma \nabla f) + R_e - R_C \tag{9}$$

where R_e is the steam generation rate, and R_c is the steam condensation rate. Eq. (9) adopts the homogeneous flow method without considering cavitation movement after steam generation. Therefore, the Rayleigh–Plesset equation is used to describe the growth of bubbles in the liquid and correctly explain the growth and collapse process of bubbles. The bubble dynamics equation is promoted as follows:

$$R_B\frac{D^2R_B}{Dt^2}+\frac{3}{2}\left(\frac{DR_B}{Dt}\right)^2=\frac{p_B-p}{p_l}-\frac{4\mu_l}{\rho_l R_B}R_B-\frac{2\sigma}{\rho_l R_B} \tag{10}$$

where R_B is the radius of the bubble; p_B is the internal pressure of the drum (assumed to be the vapor pressure at the liquid temperature when no other gas exists); p is the pressure around the bubble in the liquid; σ is the surface tension coefficient between the liquid and the vapor.

The two-phase continuity equations (liquid phase Eq. (11) and vapor phase Eq. (12)) are used to obtain an expression for the net phase change rate:

$$\frac{\partial}{\partial t}\left[(1-\alpha)\,\rho_l\right]+\nabla\cdot\left[(1-\alpha)\,\rho_l\vec{V}\right]=-R \tag{11}$$

$$\frac{\partial}{\partial t}(\alpha\rho_v)+\nabla\cdot(\alpha\rho_v\vec{V})=R \tag{12}$$

where R is the net phase transition rate, and its value is $R_e - R_c$.

According to Eqs. (11) and (12), the mixed flow equation is obtained as follows:

$$\frac{\partial}{\partial t}(\rho)+\nabla\cdot(\rho\vec{V})=0 \tag{13}$$

According to Eqs. (11)–(13), the relationship between the mixing density ρ and the steam volume fraction α can be obtained:

$$\frac{D\rho}{Dt}=-(\rho_l-\rho_v)\frac{D\alpha}{Dt} \tag{14}$$

The vapor volume fraction α is

$$\alpha=n\frac{4}{3}\pi R_B^3 \tag{15}$$

where n is the number of vacuoles. Therefore, substituting Eq. (15) into Eq. (14),

$$\frac{D\rho}{Dt}=-(\rho_l-\rho_v)(n4\pi)^{\frac{1}{3}}(3\alpha)^{\frac{2}{3}}\frac{DR_B}{Dt} \tag{16}$$

For Eq. (10), if the surface tension term and the viscous damping term are combined with Eqs. (11), (12), (14), and (16), the expression of the net phase change rate R can be obtained as follows:

$$R=(n4\pi)^{\frac{1}{3}}(3\alpha)^{\frac{2}{3}}\frac{\rho_v\rho_l}{\rho}\left[\frac{2}{3}\left(\frac{P_B-P}{\rho_l}\right)-\frac{2}{3}R_B\frac{D^2R_B}{Dt^2}\right]^{\frac{1}{2}} \tag{17}$$

Combining Eqs. (9) and (17) (ignoring the second derivative of R_B mainly in the initial bubble acceleration process), the new steam transport equation can be expressed as:

$$\frac{\partial}{\partial t}(\rho f)+\nabla\cdot\left(\rho\vec{V}f\right)=(n4\pi)^{\frac{1}{3}}(3\alpha)^{\frac{2}{3}}\frac{\rho_v\rho_l}{\rho}\left[\frac{2}{3}R_B\left(\frac{P_B-P}{\rho_l}\right)\right]^{\frac{1}{2}} \tag{18}$$

The right half of Eq. (18) is expressed as the steam generation rate.

When $P_B - P < 0$, $\frac{P_B-P}{\rho_l}$ takes the absolute value; Eq. (18) represents the cavitation collapse or generation process.

When the saturated vapor pressure P_B equals the saturated vapor pressure when there is no dissolved gas, mass transport, and viscous damping, $P_B = P_v$, Eq. (18) is called the Foam reduction kinetic formula. In Eq. (18), except for n, the other phases are known or are dependent variables. When ignoring the general model of the bubble number density, the phase transition rate formula is expressed by the bubble radius R_B as follows:

$$R_e = \frac{3\alpha}{R_B}\frac{\rho_v\rho_l}{\rho}\left[\frac{2}{3}\frac{p_v - p}{\rho_l}\right]^2 \tag{19}$$

For simplicity, let R_B be the maximum possible cavity radius; R_B is determined by the balance between aerodynamic drag and surface tension:

$$R_B = \frac{0.061 W_e \sigma}{2\rho_l v_{rel}^2} \tag{20}$$

V_{rel} is usually approximately 5% –10% of the fluid velocity using the limit parameters, e.g., RB→0 as $\alpha \to 0$. The phase change rate per unit volume is proportional to the parent term of the phase change, and the steam generation rate R_e and the condensation term R_c can be obtained by expressing the steam mass fraction i as follows:

$$R_e = C_e \frac{V_{ch}}{\sigma}\rho_l\rho_v\left[\frac{2}{3}\frac{P_v - P}{\rho_l}\right]^{\frac{1}{2}}(1-f) \tag{21}$$

$$R_c = C_c \frac{V_{ch}}{\sigma}\rho_l\rho_v\left[\frac{2}{3}\frac{P - P_v}{\rho_l}\right]^{\frac{1}{2}} f \tag{22}$$

In Eqs. (21) and (22), V_{ch} is the characteristic velocity (relative velocity between liquid and vapor); C_e and C_c are empirical coefficients. These relationships are based on certain assumptions: 1) in the bubble flow state, the phase change rate is proportional to the square of the characteristic velocity V_{ch}, but the phase change rate and the velocity are linearly related in most practical conditions of two-phase flow; 2) the relative velocity between the liquid phase and the atmosphere is 1%–10% of the average velocity. The local turbulent velocity fluctuations are also around this range in most turbulent flows. Therefore, V_{ch} can be approximated as a practical substitute for the square root $\sqrt{k}$ of the local turbulent kinetic energy.

Through cavitation coefficient analysis, the main factors affecting cavitation, such as fluid pressure, velocity, etc., are determined to provide a theoretical basis for optimizing boundary operating conditions. Based on the basic equations of fluid dynamics and turbulence models (standard κ-ε model, RNG κ-ε model, κ-w model group, SST κ-w model, etc.), combined with the external flow characteristics of the meshing herringbone gear pump, it is determined to use the RNG κ-ε turbulence model for simulation. The features of the cavitation model are analyzed, and the cavitation simulation of the pump adopts the Full cavitation model based on the Rayleigh-Plesset equation and bubble dynamics. Based on the above analysis results, a theoretical foundation is laid for simulating the external herringbone gear pump.

3 Numerical Model

3.1 Mesh Division

Table 1 lists the external meshing herringbone gear pump of main parameters, and Fig. 1a shows the 3D model and the section view. The calculation area is depicted in Fig. 1b, comprising primarily

the inlet and outlet regions, as well as the rotating fluid area. The external meshing herringbone gear pump is simplified, and the flow path area is obtained using Ansys software, as shown in Fig. 2. The calculation area of the simulation is divided mainly into stator area (A1 and A2) and rotor area (A3 and A4). The monitoring points at the inlet channel (Points 1 and 2), meshing area (Points 3 and 4), and outlet channel (Points 5 and 6) are set to obtain various parameters more intuitively, as shown in Fig. 2.

Table 1: Main parameters of an external meshing herringbone gear pump

Name	Numerical value
Rated speed (RPM)	5000
Tooth number	6
Tooth width (mm)	478
Addendum diameter (mm)	210.52
Gear center distance (mm)	180

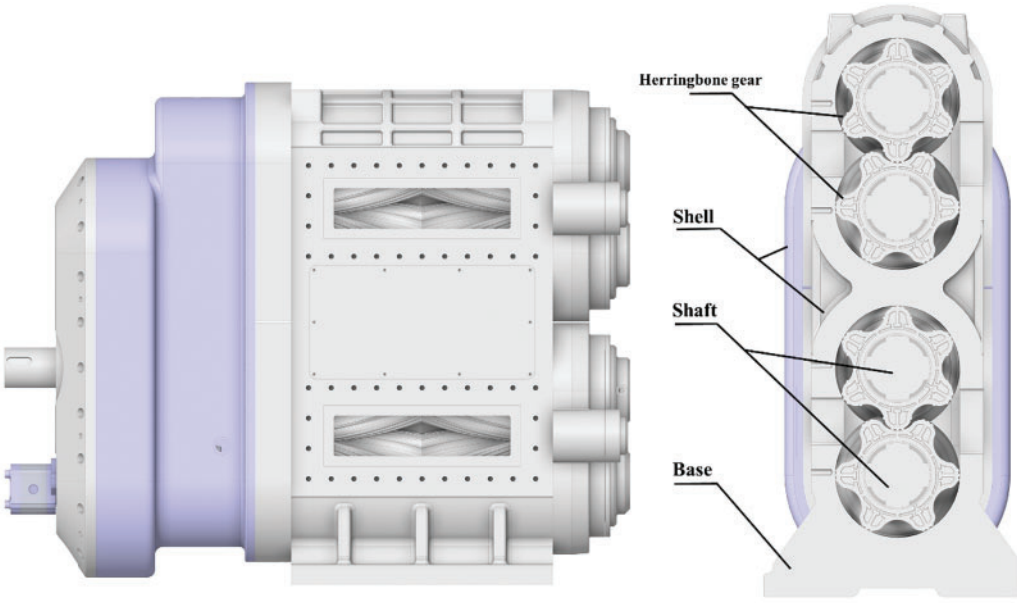

(a) 3D model and Section view of the external herringbone gear pump.

Figure 1: (Continued)

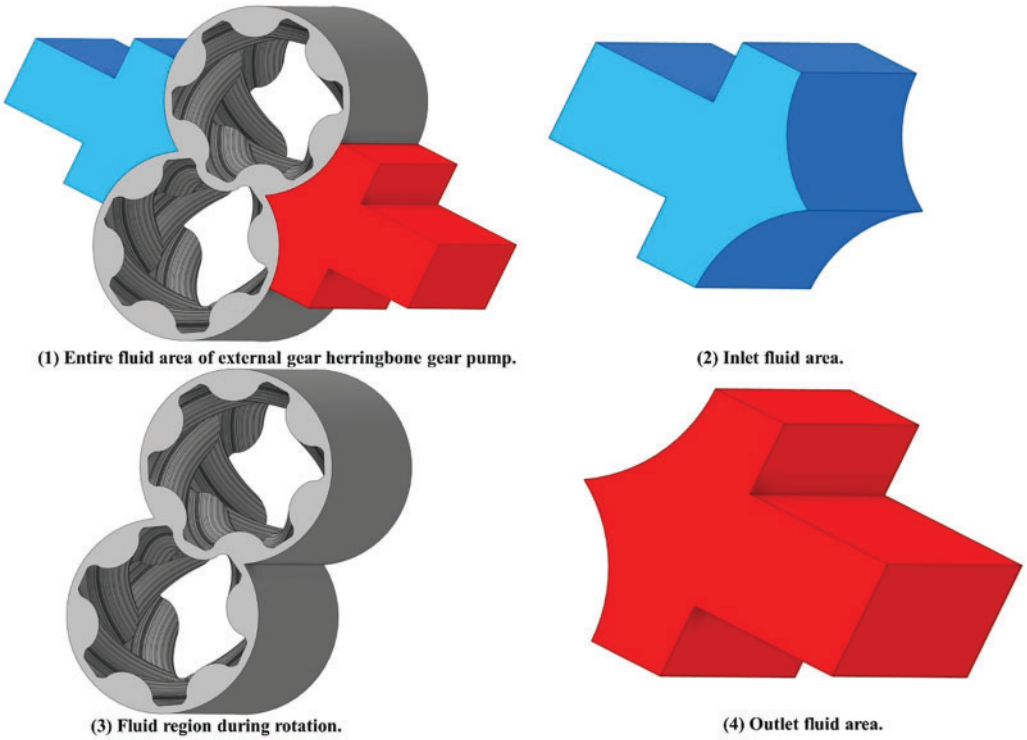

Figure 1: (a) 3D model and section view of the external herringbone gear pump and (b) Fluid calculation area of the external herringbone gear pump

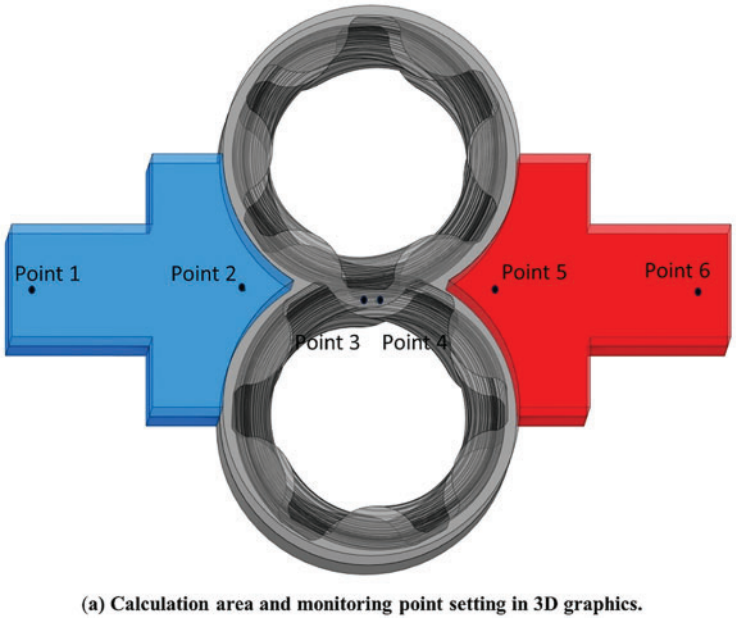

Figure 2: (Continued)

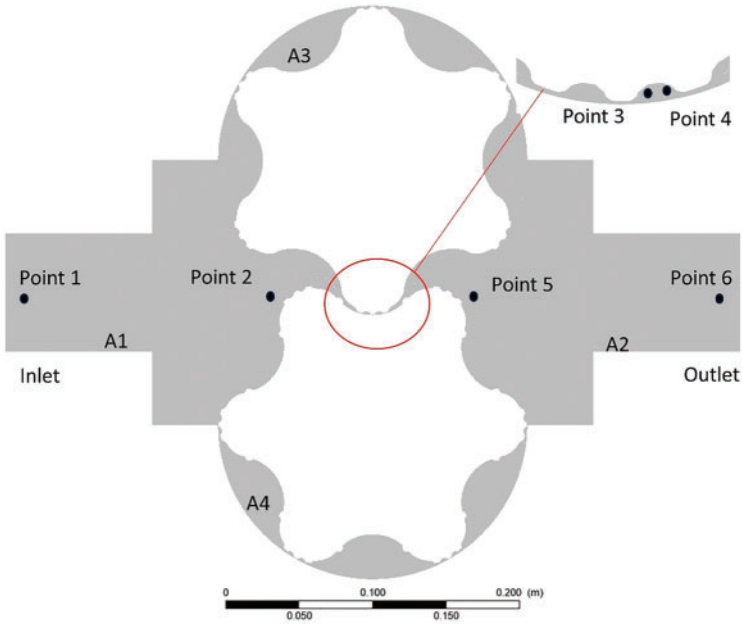

(b) Calculation area and monitoring point setting at center section in xy plane.

Figure 2: Calculation area and monitoring point setting of the external meshing herringbone gear pump in 3D graphics (a) and at center section in xy plane (b)

For the grid division of the rotor area, TwinMesh software is used to obtain high-quality hexahedral grids, improve grid resolution, and describe flow field boundary layer flow and gap flow. The meshing process using TwinMesh is as follows:

① Use Ansys SpaceClaim to obtain the rotor curve (IGES or ASCII file) from the rotor end face and import it into TwinMesh.

② Use TwinMesh first to obtain the meshing curve (as shown in Fig. 3a) and then generate a 2D grid (as shown in Fig. 3b).

③ Check the grid quality–the minimum grid angle needs to be greater than 18° to meet the requirements (as shown in Fig. 4a), generate a 3D grid, and check the grid quality (as shown in Fig. 4b). Table 2 lists its main parameter settings.

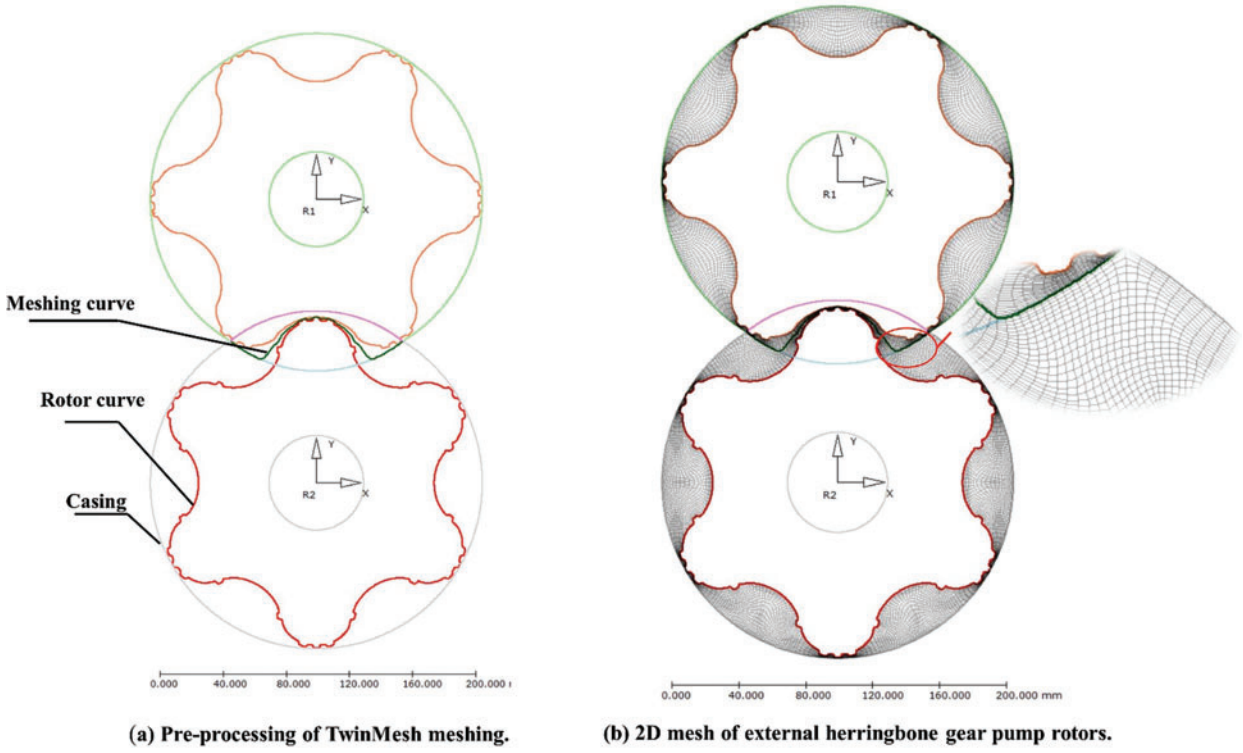

(a) Pre-processing of TwinMesh meshing. (b) 2D mesh of external herringbone gear pump rotors.

Figure 3: (a) Pre-processing of TwinMesh meshing and (b) 2D mesh of external herringbone gear pump rotors

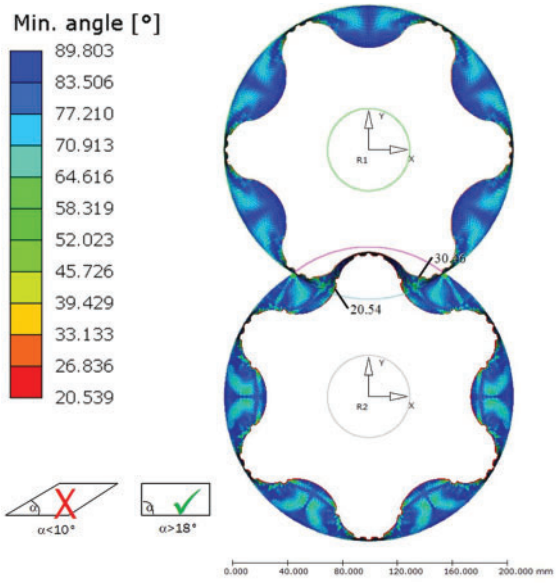

(a) Mesh quality check of external herringbone gear pump rotors.

Figure 4: (Continued)

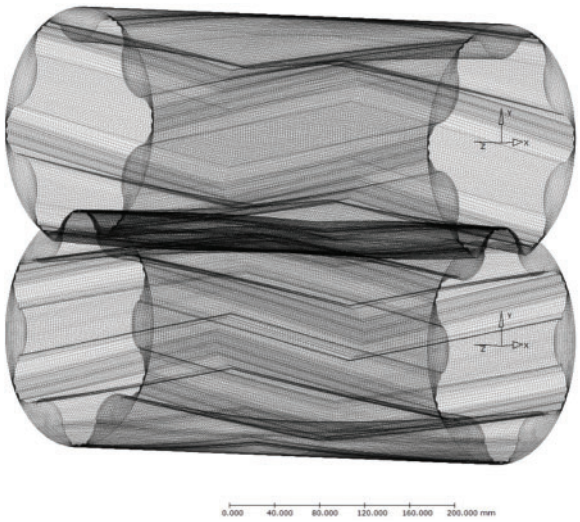

(b) 3D mesh of external herringbone gear pump rotors.

Figure 4: (a) Mesh quality check of external herringbone gear pump rotors and (b) 3D mesh of external herringbone gear pump rotors

Table 2: Setting of main parameters of rotor meshing of external meshing herringbone gear pump

Option	Content	Value
Mesh	Type of meshing	InnerFix
	Use properties for rotors	Identically
	Maximum element size (mm)	2
Boundary layer refinement	First element height (inner)(mm)	0.5
	First element height (outer)(mm)	0.5
Number of elements	Number of elements (radial)	25
	Number of elements in z-direction	160
	Type of node distribution in Z	Uniform
	Elements in axial gap MZ	5
	Elements in axial gap PZ	5

The mesh of the stator area uses Ansys meshing software, and the maximum mesh size is 2 mm. Combining the divided stator area mesh with the rotor area mesh, Table 3 lists the export settings, and the cavitation model is set to the Rayleigh–Plesset model. Fig. 5 shows the derived computational domain grid.

Table 3: Statistical situation of grid division in the computational domain of external meshing herringbone gear pump

Numbering	Maximum grid size	Number of elements	Number of nodes
1	1	6,350,126	6,655,584
2	1.5	5,150,126	5,399,784
3	2	4,430,126	4,646,304
4	3.2	3,998,126	4,194,216

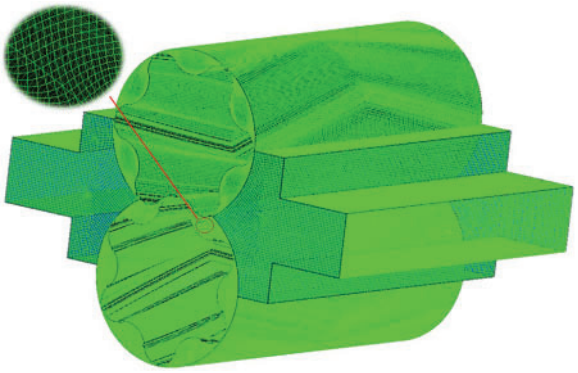

Figure 5: 3D mesh of external herringbone gear pump

3.2 Grid Independence Verification

Grid quality and quantity significantly influence the CFD simulation results. Therefore, independence verification is required to ensure the simulation accuracy. "Grid independence" means that in numerical simulation, the simulation results are unaffected by grid resolution and shape; the simulation results obtained on different grids are similar. Grid independence verification is performed by changing the grid size [50–52]. Only the grid size is reversed, keeping other conditions unchanged, and the number of grids obtained in turn is 3,998,126, 4,430,126, 5,150,126, and 6,350,126. Additional information is listed in Table 3. The simulation is carried out under different grid numbers, and the head of the external meshing herringbone gear pump is obtained, as shown in Fig. 6. The head of the water pump is approximately 204.593 m, and the maximum head error of the four simulations is 0.003% (the error is less than 3%, so the simulation can be considered valid). Hence, the simulation results have nothing to do with the number of grids. The simulation results are quite different from the other three groups when the maximum grid size is 3.2 mm (the number of grids is 3,998,126) (Fig. 6). Thus, the grid accuracy does not meet the simulation requirements. To save simulation time and reduce simulation cost, the maximum grid size is 2 mm, and the number of grids is 4,430,126 for cavitation simulation.

The computational domain mesh is generated using a meshing method with a maximum mesh size of 2 mm. The speed used in the simulation was 5000 RPM, with the inlet and outlet pressures set to 1 bar and 20 bar, respectively. The inlet temperature was set to 293.15 K. The RNG κ-ε turbulence model and the Full cavitation model were employed in the CFX simulation. The simulation is completed based on the above settings. The maximum value of the residual is set to 1.0e-3, and the residual is monitored. The residual result is stable, and the ultimate residual result is 2.57e-4. Therefore, the simulation converges, and the simulation result is reliable.

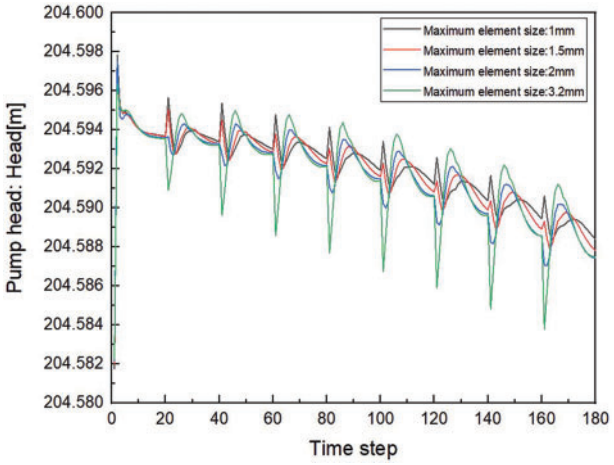

Figure 6: Verification of grid independence of the external meshing herringbone gear pump simulation

4 Results and Discussion

The simulated head and experimental head changes of the external meshing herringbone gear pump at different speeds are shown in Fig. 7. As shown in Fig. 7, the errors between the simulated and experimental displacements at four different speeds are 4.9%, 4.8%, 3.6%, and 2.6%, respectively. The simulation results are lower than the calculation results because the calculation results do not consider lateral clearance leakage [53,54]. The error between the experiment and simulation results is less than 5%. The calculation model is valid, and the simulation results are credible.

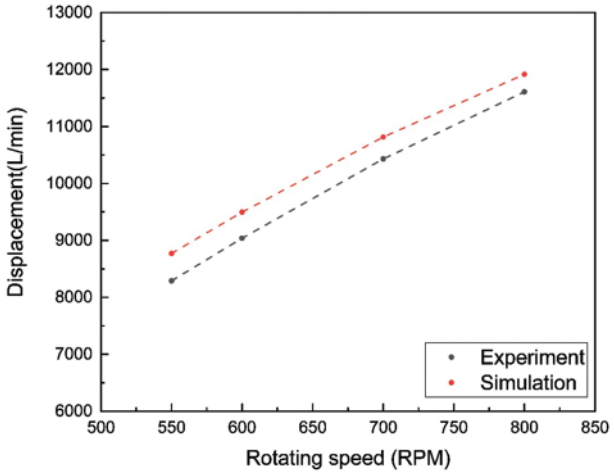

Figure 7: Experimental displacement and simulated displacement at the outlet

4.1 Effect of Cavitation on External Meshing Herringbone Gear Pump

The cavitation simulation results of the external meshing herringbone gear pump indicate that the most serious cavitation phenomenon occurs in the meshing area (Fig. 8). Fig. 8a provides an overview of the cavitation situation in the herringbone external gear pump. Figs. 8b–8d show section views along the axial direction and the changes are consistent. The severe cavitation areas are mainly distributed

in the meshing area. Fig. 9 shows the change in gas volume fraction at the monitoring point around the meshing area. The gas volume fraction of Points 3 and 4 in the meshing area is above 70% (Fig. 9), which is consistent with the analysis results in Fig. 8. In other monitoring points with the regular operation of the external mesh herringbone gear pump, the pressure tends to be stable, and the gas volume fraction tends to be zero. Fig. 10 shows the pressure distribution diagram of the central section obtained at a particular moment. The pressure distribution of the flow channel is uniform, and the pressure change area is distributed near the meshing area.

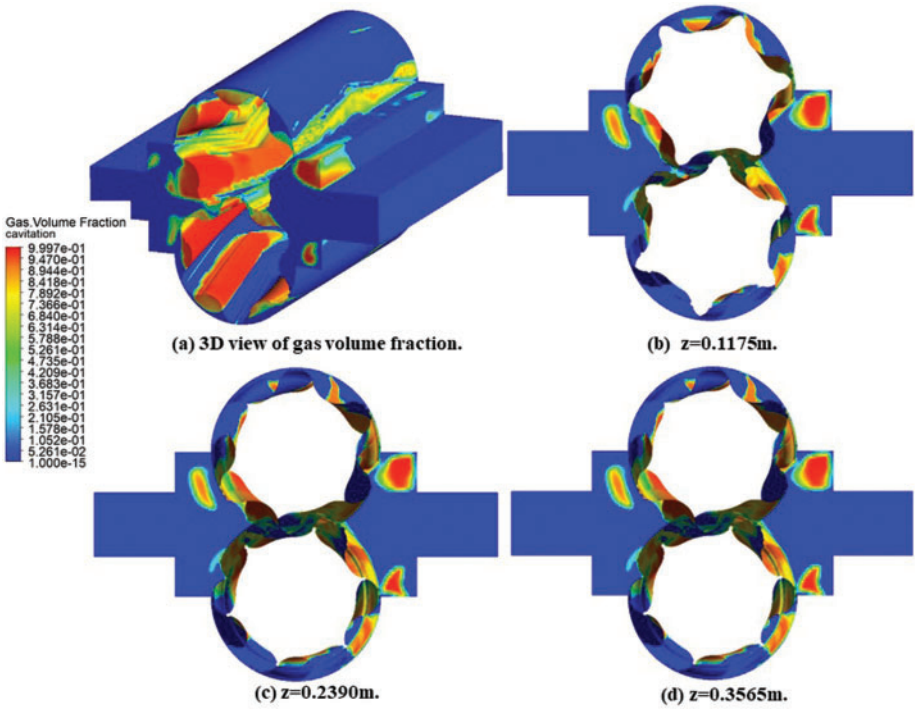

Figure 8: Gas volume fraction in the internal flow field of the external meshing herringbone gear pump

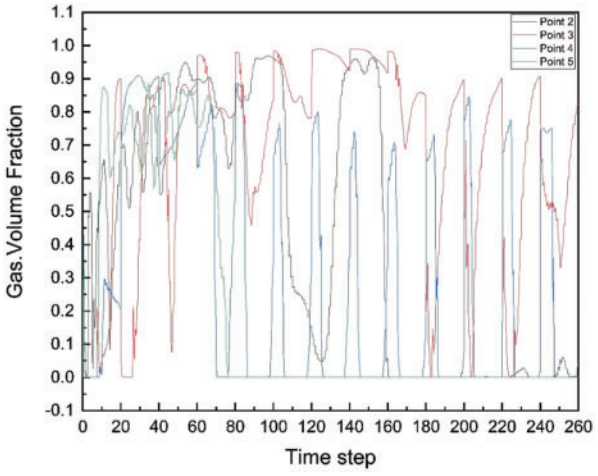

Figure 9: Changes in the gas volume fraction at each monitoring point

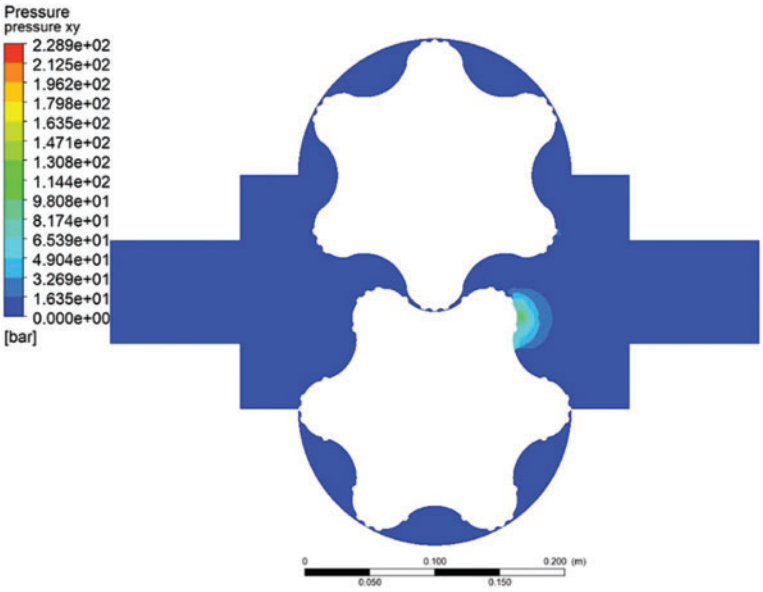

Figure 10: Central cross-sectional pressure distribution map at 0.026 s

Figs. 11a and 11b show the pressure pulsation and speed change of Points 1, 4, and 6. Fig. 11 shows that the pressure pulse at Point 4 is large, and the speed changes quickly. Hence, it will impact the rotor, resulting in vibration and noise. Based on the above analysis, Point 4 is an important monitoring point for the following cavitation research.

Based on the above analysis, in the case of a high-speed external meshing herringbone gear pump, cavitation occurs mainly in the meshing and meshing gap areas (as shown in Fig. 8). Pressure shocks (as shown in Fig. 11a, pressure changes at Point 4) may cause abnormal meshing of the gear teeth and increase wear, whereas cavitation can also cause wheel corrosion and tooth surface erosion [55]. Therefore, more wear-resistant and corrosion-resistant materials should be selected in the manufacturing process of rotor gears. Cavitation causes flow pulsation at the outlet, as shown in Fig. 7.

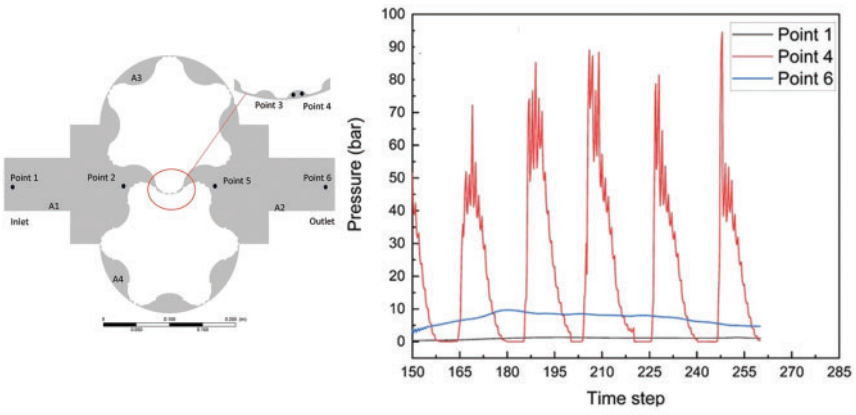

(a) Point 1, Point 4, and Point 6 pressure measurement results.

Figure 11: (Continued)

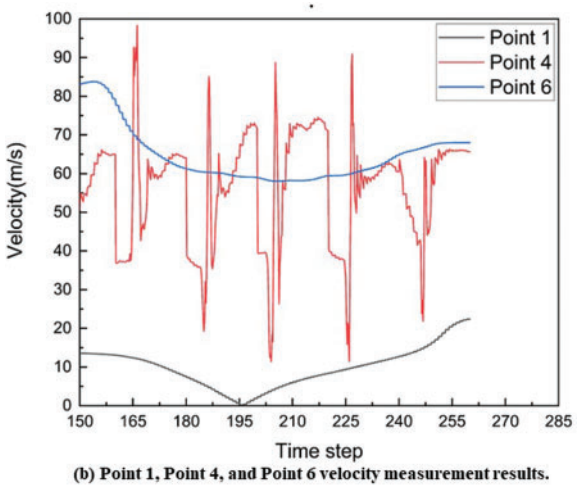

(b) Point 1, Point 4, and Point 6 velocity measurement results.

Figure 11: Point 1, Point 4 and Point 6 pressure and velocity monitoring results

Among the basic parameters of externally meshing herringbone gears, the helix angle is one of the critical factors affecting the pressure distribution in the pump and the liquid flow mode. Therefore, the helix angle is selected as the primary research object in terms of the influence of the gear shape on cavitation. In addition, the operating conditions (mainly fluid temperature, pressure, properties, gas content, speed, load, and working conditions) should be optimized to reduce the impact of cavitation on the external gear pump. The pump must have a high speed and outstanding displacement characteristics because the external meshing herringbone gear pump is a flood discharge type, and it is difficult to change the working conditions and various parts of the fluid. Therefore, this study chooses the speed and inlet pressure as the research object of the optimized working condition.

4.2 Influence of Rotational Speed on Cavitation

The rotational speed is changed, with the other conditions unchanged. Different speeds (3000 RPM, 5000 RPM, and 7000 RPM) are set to study the cavitation characteristics of the external meshing herringbone gear pump, and Fig. 12 shows the simulation results. Cavitation is more serious when the speed increases [56,57], as shown in Figs. 12a–12c. A comparison of Figs. 12b and 12c show that the rate increased to 7000 RPM. Moreover, in addition to the meshing gap area, the cavitation phenomenon at the inlet channel is intensified; Fig. 13a shows the pressure change. The gas volume fraction of Point 4 increases as the speed increases, as shown in Fig. 13b. Therefore, the cavitation in the meshing area becomes serious, which is consistent with the simulation results in Fig. 12. For the external meshing herringbone gear pump, the speed and the fluid flow rate are increased, keeping the other parameters unchanged. According to Eq. (1), a smaller cavitation value σ means that it is easier to cause cavitation. At the same time, a higher velocity will lead to a more obvious pressure drop in the fluid system, making it easier for the local pressure to drop below the vapor pressure of the liquid, and the formation and rupture of cavitation bubbles are more frequent and intense. Therefore, the pressure drop between the rotor area and the inlet channel increases, and the cavitation phenomenon in the inlet channel intensifies.

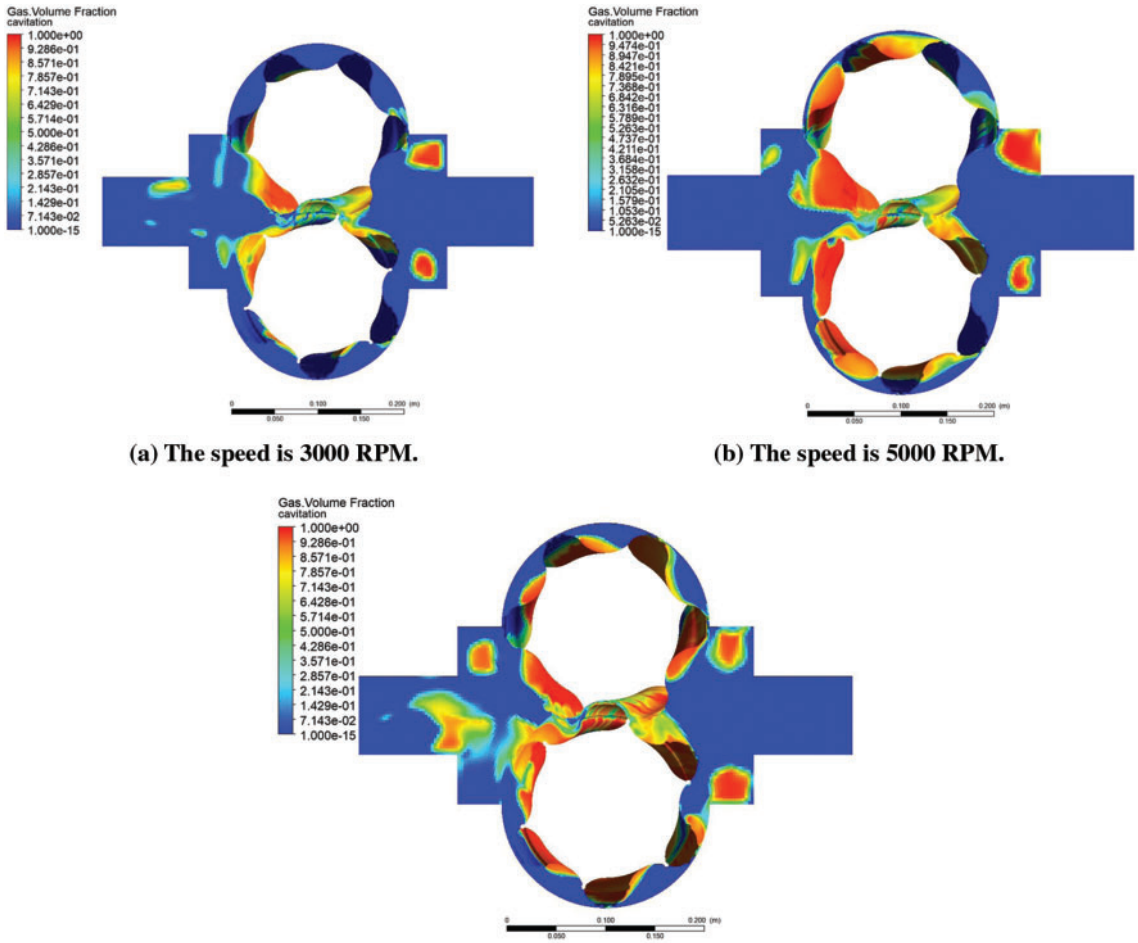

(a) The speed is 3000 RPM.

(b) The speed is 5000 RPM.

(c) The speed is 7000 RPM.

Figure 12: Cavitation simulation results at different speeds

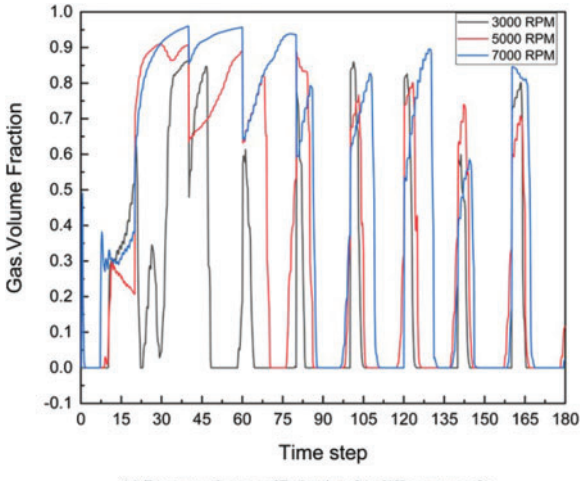

(a) Pressure change of Point 4 under different speeds.

Figure 13: (Continued)

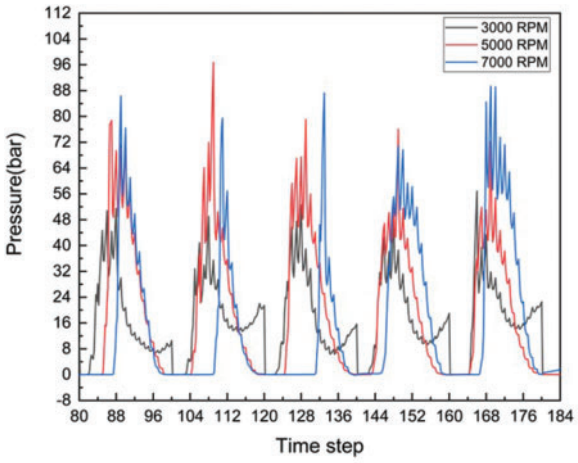

(b) Gas volume fraction of Point 4 under different speeds.

Figure 13: Point 4 Pressure and gas volume fraction at different speeds

4.3 Influence of Inlet Pressure on Cavitation

The inlet pressure is changed, with the other conditions unchanged. The inlet pressure is set to 1 bar, 3 bar, and 5 bar. Fig. 14 shows the simulation results. Figs. 14a–14c show that the severe cavitation area is reduced significantly. According to Eq. (1), the cavitation number σ increases as the pressure of the fluid increases, and cavitation is less likely to occur. Increasing the inlet pressure of the pump can reduce the gas entering the pump [58] and increase the pressure difference between the saturated vapor pressure of the liquid and the gas so that the fluid pressure is not quickly lower than the saturated vapor pressure. Figs. 15a and 15b show the change in pressure and gas volume fraction of Point 4 in the meshing region. According to Figs. 15a and 15b, the inlet pressure increases, and the pressure at Point 4 does not change significantly, but the gas volume fraction decreases. When the inlet pressure is 5 bar, the gas volume fraction after 0.0105 s (Step time = 0.0001 s) is <50%, suggesting that the cavitation phenomenon is weakened at an inlet pressure of 1 and 3 bar.

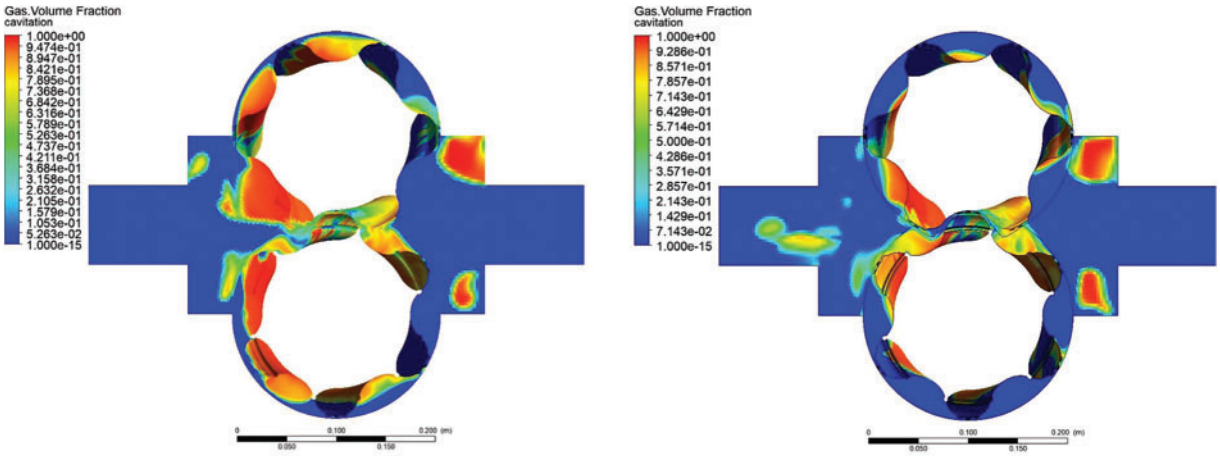

(a) Inlet pressure is 1 bar. (b) Inlet pressure is 3 bar.

Figure 14: (Continued)

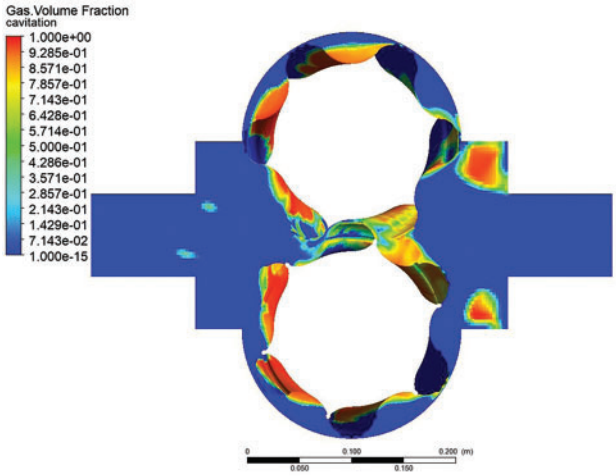

(c) Inlet pressure is 5 bar.

Figure 14: Cavitation simulation results of external herringbone gear pumps under different inlet pressures

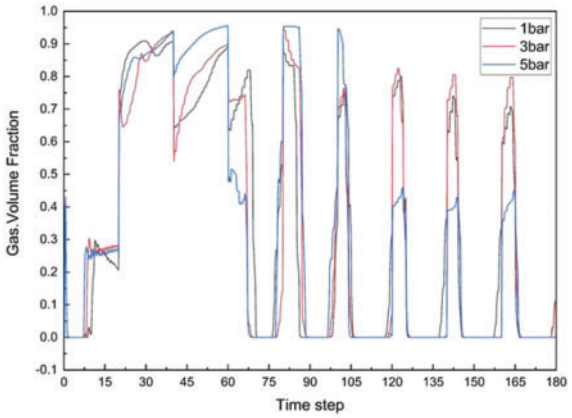

(a) Gas volume fraction of Point 4 under different inlet pressure.

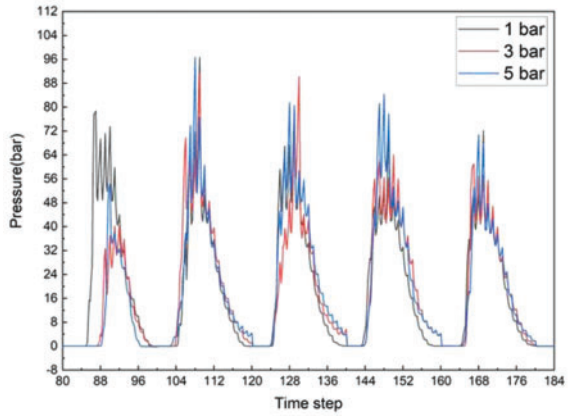

(b) Pressure change of Point 4 under different inlet pressure.

Figure 15: Pressure and gas volume fraction of Point 4 at different inlet pressures

4.4 Influence of Helix Angle on Cavitation

The helix angle of the rotor gear is changed with the other conditions kept constant. Figs. 16a–16c show the cavitation simulation results at helix angles of 24°, 27°, and 30°, respectively. According to Figs. 16a–16c, in the external meshing herringbone gear pump meshing clearance area, the helix angle and the degree of cavitation decrease. According to Fig. 17b, it can be seen that the pressure change trend of the meshing point Point 4 is the same under different helix angles, but the pressure impact intensity is different. It can be seen from Fig. 17a that in the stable operation stage (t = 0.0165 s), the gas volume fraction at Point 4 is more significant than 70%, but the smaller the spiral angle, the more serious the cavitation phenomenon. When the helix angle is 24°, the gas volume fraction is approximately 90%. To analyze pressure changes and gas volume fraction, we selected the maximum and minimum pressure values to determine the maximum pressure difference and average gas volume fraction at Point 4 for different helix angles (refer to Fig. 18). As the helix angle increases, the overall pressure change within the same period gradually decreases. This indicates a smaller difference between the maximum and minimum pressure values, suggesting a gradual decrease in maximum pressure impact. This is advantageous for improving the meshing process, enhancing fluidity and lubricity, and reducing the squeezing effect. For different helix angles, the average gas volume fractions at Point 4 during one rotation of the rotor are 34.4% (24°), 23.1% (27°), and 19.0% (30°). Consequently, as the helix angle increases, the average gas volume fraction decreases, resulting in a weakening of cavitation. This can be attributed to the fact that a higher gear helix angle β leads to a greater tooth surface coincidence degree ε, which improves lubrication and fluidity during the meshing process, reduces the squeezing effect, and enhances resistance to gas leakage. As a result, the possibility of squeezing and cavitation is reduced. The changing trend observed in the simulation results aligns with the findings of the theoretical analysis. Based on the above analysis, reducing the helix angle can reduce the occurrence of severe cavitation areas. The cavitation gas volume fraction will increase during the gear meshing process, and the probability of cavitation will increase.

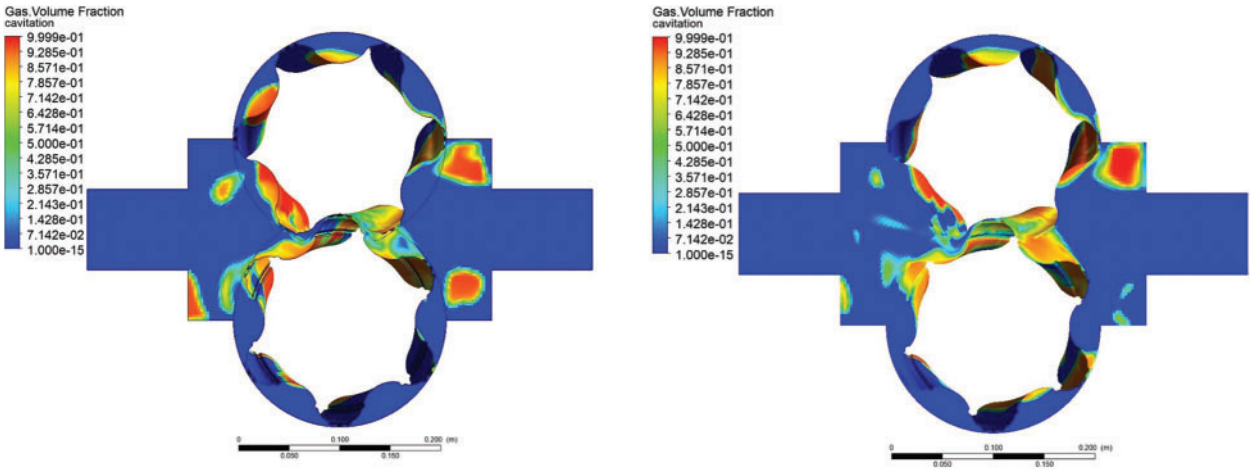

(a) The helix angle is 24°. **(b) The helix angle is 27°.**

Figure 16: (Continued)

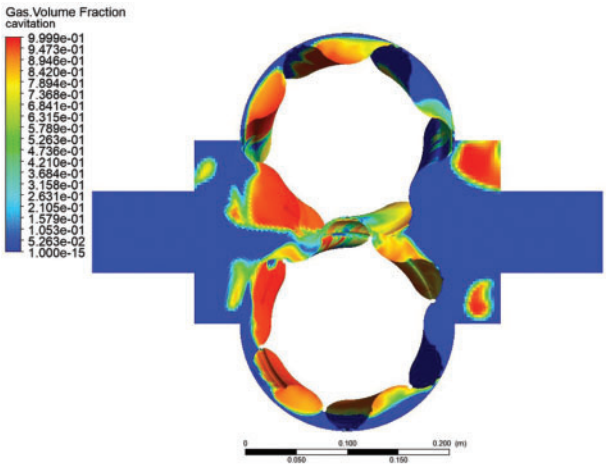

(c) The helix angle is 30°.

Figure 16: Cavitation simulation results of external herringbone gear pump with different helix angles

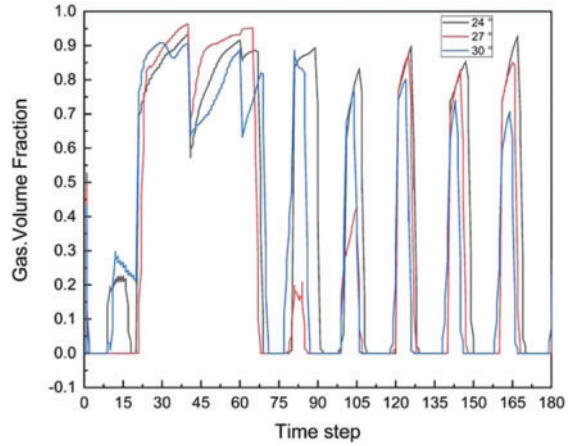

(a) Gas volume fraction of Point 4 under different helix angles.

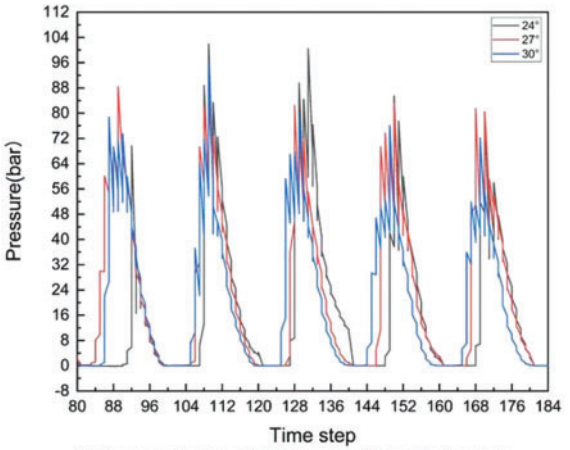

(b) Pressure change of Point 4 under different helix angles.

Figure 17: Pressure and gas volume fraction of Point 4 at different helix angles

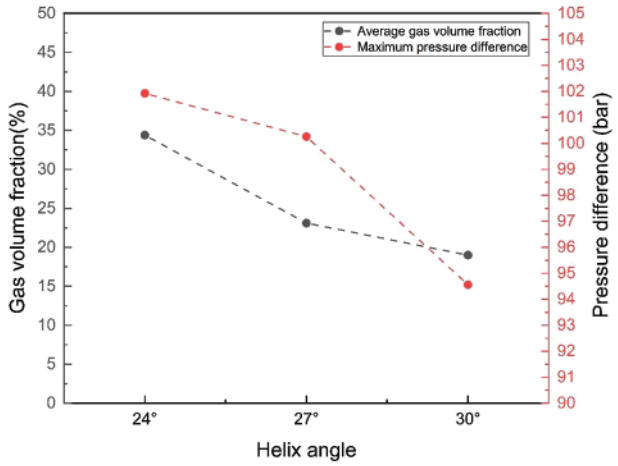

Figure 18: Average gas volume fraction and maximum pressure difference at Point 4 under different spiral angles during the same period

CFD (Computational Fluid Dynamics) is a valuable tool for researchers to gain a better understanding of fluid systems and optimize their performance [59–61]. In this particular study, cavitation is observed primarily in the meshing area and the meshing gap area of the external meshing herringbone gear pump, as depicted in Fig. 8. The occurrence of cavitation is found to be significantly influenced by factors such as speed, inlet pressure, and helix angle, as illustrated in Figs. 13–17. By utilizing CFD, researchers can visually investigate cavitation, gain insights into its underlying mechanism, and identify the specific regions where it occurs. Moreover, CFD analysis provides valuable guidance for optimizing the performance of the external meshing herringbone gear pump. Simulation results for various design schemes demonstrated that appropriate adjustment of design parameters can effectively reduce or eliminate cavitation.

5 Conclusion

For the research on the cavitation characteristics of the external meshing herringbone gear pump, TwinMesh is first used to obtain a high-quality hexahedral mesh to reduce the oscillation or numerical dissipation caused by the mesh quality, improve the simulation quality, and avoid the shape caused by the tetrahedral mesh distortion and node irregularities. TwinMesh is combined with the CFX solver to complete the simulation. An analysis of the principle of cavitation is determined in a numerical simulation using the RNG κ–ε turbulence model and the Full cavitation model. The grid size is changed to ensure the simulation accuracy, and the simulation is carried out with the number of grids 3,998,126, 4,430,126, 5,150,126, and 6,350,126. The obtained head is approximately 204.593 m, and the maximum error is 0.003%. The simulation result has nothing to do with the number of grids. The error between the experiment and simulation results is less than 5%. Therefore, the calculation model is valid, and the simulation results are credible. At the same time, monitoring points are set up during the simulation process to determine changes in pressure, gas volume fraction, etc., in the inlet channel, meshing area, and outlet channel and analyze the flow conditions in the pump. These results provide better support for the study of cavitation phenomena. The factors affecting cavitation (speed, inlet pressure, and helix angle) are determined by analyzing the cavitation number equation. Numerical simulations are carried out. Point 4 in the meshing area is taken as an essential monitoring point, and the following conclusions can be drawn:

① The severe cavitation area of the external meshing herringbone gear pump is distributed mainly in the meshing gap and meshing area. After t = 0.0165 s, the gas volume fraction in the meshing area (Points 3 and 4) is higher than 80%, resulting in cavitation. The volume fraction of inlet channels (Points 1 and 2) and outlet channels (Points 5 and 6) is less than 10%. Cavitation causes a specific pulsation in the outlet flow.

② In the case of high speed (3000 RPM, 5000 RPM, and 7000 RPM), cavitation is reduced significantly when the rate is reduced. In particular, in the case of 7000 RPM, the place where the gas volume fraction of the inlet channel is more significant than 50% increases significantly. The gas volume fraction in the meshing area (Point 4) is above 65% at three speeds, and cavitation occurred. Cavitation can be reduced by reducing the rotational speed.

③ Under different inlet pressures (1 bar, 3 bar, and 5 bar), cavitation is reduced significantly when the inlet pressure is increased. In particular, for the meshing area (Point 4), when the inlet pressure is 5 bar, after t = 0.0105 s, the gas volume fraction is lower than 45%, which reduces cavitation. Increasing the inlet pressure is an effective way of reducing the occurrence of cavitation.

④ Under different helix angles (24°, 27°, and 30°), reducing the helix angle can effectively reduce the area where cavitation occurs. In the stable operation stage (t = 0.0165 s), the gas volume fraction at Point 4 is more significant than 70%, but the smaller the spiral angle, the more serious the cavitation phenomenon. When the helix angle is 24°, the gas volume fraction is approximately 90%. This is different from the cavitation simulation results in other areas. As the helix angle increases, the tooth surface coincidence becomes larger. Within the same rotation period, the average gas volume fraction and maximum pressure difference at Point 4 are reduced, and the cavitation imagination is improved. Therefore, the selection of the helix angle needs to consider the influence of cavitation during the gear meshing process. In the selection of parameters and boundary conditions for the external meshing herringbone gear pump, several factors need to be considered. These include the rotation speed, inlet pressure, and helix angle. It is important to choose a lower speed to minimize the occurrence of cavitation during the meshing process and in the meshing area, while ensuring the desired outlet flow and pressure. Increasing the inlet pressure can also help reduce the occurrence of cavitation by reducing the areas where it can happen. The helix angle plays a dual role in cavitation prevention. Lowering the helix angle can help reduce cavitation in the meshing area, while increasing it can help reduce cavitation during the meshing process. Therefore, increasing the helix angle can improve fluidity and lubricity, reduce decompression, and reduce cavitation generation during the meshing process. However, it is necessary to balance this with the need to increase inlet pressure or decrease rotation speed to mitigate the impact of cavitation around the meshing area. To enhance stability and extend the service life of the outer meshing herringbone gear rotor, a synthetic material coating that can withstand changes in pressure, speed, and liquid properties can be applied to the material surface. It is important to note that factors such as fluid temperature, viscosity, and flow path also influence cavitation, but were not separately studied in this research. These factors should be considered in future studies. The findings of this research provide valuable insights for selecting parameters and boundary conditions for the external meshing herringbone gear pump, to minimize the impact of cavitation.

Acknowledgement: The authors thank the support from the Grant (2024-MOIS35-005) of Policy-linked Technology Development Program on Natural Disaster Prevention and Mitigation funded by Ministry of Interior and Safety (MOIS, Korea).

Funding Statement: This research was supported by a Grant (2024-MOIS35-005) of Policy-linked Technology Development Program on Natural Disaster Prevention and Mitigation funded by Ministry of Interior and Safety (MOIS, Korea).

Author Contributions: The authors confirm contribution to the paper as follows: study conception and design: Chul-Hee Lee, Jinlong Yang; data collection: Jinlong Yang, Kwang-Hee Lee; analysis and interpretation of results: Jinlong Yang, Kwang-Hee Lee, Chul-Hee Lee; draft manuscript preparation: Jinlong Yang, Kwang-Hee Lee, Chul-Hee Lee. All authors reviewed the results and approved the final version of the manuscript.

Availability of Data and Materials: Data and materials can be obtained through the corresponding author's email address.

Conflicts of Interest: The authors declare that they have no conflicts of interest to report regarding the present study.

References

1. Kranenburg, C. (1974). Gas release during transient cavitation in pipes. *Journal of the Hydraulics Division, 100(10),* 1383–1398.
2. Christopher, S., Kumaraswamy, S. (2013). Identification of critical net positive suction head from noise and vibration in a radial flow pump for different leading edge profiles of the vane. *Journal of Fluids Engineering, 135(12),* 121301.
3. Liu, X., Chen, X., Kang, R., Shen, X., Ni, B. (2020). A coupled cavitation model in an oscillatory oil squeeze film. *Computer Modeling in Engineering Sciences, 123(1),* 129–152. https://doi.org/10.32604/cmes.2020.07836
4. Kan, K., Binama, M., Chen, H., Zheng, Y., Zhou, D. et al. (2022). Pump as turbine cavitation performance for both conventional and reverse operating modes: A review. *Renewable and Sustainable Energy Reviews, 168,* 112786.
5. Binama, M., Muhirwa, A., Bisengimana, E. (2016). Cavitation effects in centrifugal pumps–A review. *International Journal of Engineering Research and Applications, 6(5),* 52–63.
6. Abbas, M. K. (2010). Cavitation in centrifugal pumps. *Diyala Journal of Engineering Sciences, 3,* 170–180.
7. Lin, P., Hu, D., Lu, J. M., Wang, S. (2021). CFD numerical simulation of sand-contained cavitation characteristics of axial-flow pump. *Advances in Mechanical Engineering, 13(7),* 16878140211032785.
8. Chao, Q., Zhang, J., Xu, B., Huang, H., Zhai, J. (2019). Effects of inclined cylinder ports on gaseous cavitation of high-speed electro-hydrostatic actuator pumps: A numerical study. *Engineering Applications of Computational Fluid Mechanics, 13(1),* 245–253.
9. Kang, C., Mao, N., Zhang, W., Gu, Y. (2017). The influence of blade configuration on cavitation performance of a condensate pump. *Annals of Nuclear Energy, 110,* 789–797.
10. Long, Y., Zhang, Y., Chen, J. P., Zhu, R. S., Wang, D. Z. (2021). A cavitation performance prediction method for pumps: Part2-sensitivity and accuracy. *Nuclear Engineering and Technology, 53(11),* 3612–3624.
11. Yang, W., Xiao, R., Wang, F., Wu, Y. (2014). Influence of splitter blades on the cavitation performance of a double suction centrifugal pump. *Advances in Mechanical Engineering, 6,* 963197.
12. Peng, C., Tian, S., Li, G. (2018). Joint experiments of cavitation jet: High-speed visualization and erosion test. *Ocean Engineering, 149,* 1–13.
13. Zhang, S., Tian, R., Ding, K., Chen, H., Ma, Z. (2022). Numerical and experimental study in pressure pulsation and vibration of a two-stage centrifugal pump under cavitating condition. *Modern Physics Letters B, 36(1),* 2150501.

14. Zhou, L., Hang, J., Bai, L., Krzemianowski, Z., El-Emam, M. A. et al. (2022). Application of entropy production theory for energy losses and other investigation in pumps and turbines: A review. *Applied Energy, 318,* 119211.
15. Ouyang, T., Mo, X., Lu, Y., Wang, J. (2022). CFD-vibration coupled model for predicting cavitation in gear transmissions. *International Journal of Mechanical Sciences, 225,* 107377.
16. Wang, B., Wu, X., Wang, C., Zhang, Z., Sun, S. et al. (2023). Study on non-uniform internal pressure distribution of twin-screw refrigeration compressor. *International Journal of Refrigeration, 152,* 214–222.
17. Tsao, C. C., Lin, W. K., Lai, K. Y., Yavuzkurt, S., Liu, Y. H. (2023). Numerical investigation of compression and expansion process of twin-screw machine using R-134a. *Energies, 16(8),* 3599.
18. Li, W., Liu, M., Ji, L., Li, S., Song, R. et al. (2023). Study on the trajectory of tip leakage vortex and energy characteristics of mixed-flow pump under cavitation conditions. *Ocean Engineering, 267,* 113225.
19. Del Campo, D., Castilla, R., Raush, G. A., Gamez Montero, P. J., Codina, E. (2012). Numerical analysis of external gear pumps including cavitation. *Journal of Fluids Engineering, 134(8),* 081105.
20. Fu, Q., Zhang, F., Zhu, R., He, B. (2016). A systematic investigation on flow characteristics of impeller passage in a nuclear centrifugal pump under cavitation state. *Annals of Nuclear Energy, 97,* 190–197.
21. Wang, X., Wang, Y., Liu, H., Xiao, Y., Jiang, L. et al. (2023). A numerical investigation on energy characteristics of centrifugal pump for cavitation flow using entropy production theory. *International Journal of Heat and Mass Transfer, 201,* 123591.
22. Cunningham, R. G., Hansen, A. G., Na, T. Y. (1970). Jet pump cavitation. *Journal of Fluids Engineering, 92(3),* 483–492.
23. Ouyang, T., Wang, J., Mo, X., Li, Y. (2023). Vibration and cavitation in high-speed gears caused by faults. *International Journal of Mechanical Sciences, 250,* 108322.
24. Garcia, R., Hammitt, F. G. (1967). Cavitation damage and correlations with material and fluid properties. *Journal of Fluids Engineering, 89(4),* 753–763.
25. Wei, A., Yu, L., Qiu, L., Zhang, X. (2022). Cavitation in cryogenic fluids: A critical research review. *Physics of Fluids, 34(10),* 101303.
26. Spraker, W. A. (1965). The effects of fluid properties on cavitation in centrifugal pumps. *Journal of Engineering for Gas Turbines and Power, 87(3),* 309–318.
27. Aminoroayaie Yamini, O., Mousavi, S. H., Kavianpour, M. R., Safari Ghaleh, R. (2021). Hydrodynamic performance and cavitation analysis in bottom outlets of dam using CFD modelling. *Advances in Civil Engineering, 2021*, 1–14.
28. Yin, F., Kong, X., Ji, H., Nie, S., Lu, W. (2022). Research on the pressure and flow characteristics of seawater axial piston pump considering cavitation for reverse osmosis desalination system. *Desalination, 540,* 115998.
29. Song, Y., Hou, R., Liu, Z., Liu, J., Zhang, W. et al. (2022). Cavitation characteristics analysis of a novel rotor-radial groove hydrodynamic cavitation reactor. *Ultrasonics Sonochemistry, 86,* 106028.
30. Silva, P. A. S. F., Shinomiya, L. D., de Oliveira, T. F., Vaz, J. R. P., Mesquita, A. L. A. et al. (2017). Analysis of cavitation for the optimized design of hydrokinetic turbines using BEM. *Applied Energy, 185,* 1281–1291.
31. Zhu, G., Dong, S. M. (2020). Analysis on the performance improvement of reciprocating pump with variable stiffness valve using CFD. *Journal of Applied Fluid Mechanics, 13(2),* 387–400.
32. Li, G., Ding, X., Wu, Y., Wang, S., Li, D. et al. (2022). Liquid-vapor two-phase flow in centrifugal pump: Cavitation, mass transfer, and impeller structure optimization. *Vacuum, 201,* 111102.
33. Ren, Z., Li, D., Fu, X., Wang, H., Liu, J. et al. (2023). Synergistic effects of vapor and gaseous cavitation and mass-transfer mechanism in a mechanical pump. *Physics of Fluids, 35(5),* 053335.
34. Sreedhar, B. K., Albert, S. A., Pandit, A. B. (2017). Cavitation damage: Theory and measurements-A review. *Wear, 372,* 177–196.
35. Šarc, A., Stepišnik-Perdih, T., Petkovšek, M., Dular, M. (2017). The issue of cavitation number value in studies of water treatment by hydrodynamic cavitation. *Ultrasonics Sonochemistry, 34,* 51–59.

36. Jian, W. (2015). *Numerical calculation and experimental research on cavitation erosion of hydraulic equipment (Doctoral dissertation)*. Jiangsu University, China (In Chinese).
37. Guo, G., Zhang, R., Yu, H. (2020). Evaluation of different turbulence models on simulation of gas-liquid transient flow in a liquid-ring vacuum pump. *Vacuum, 180,* 109586.
38. Ahsan, M. (2014). Numerical analysis of friction factor for a fully developed turbulent flow using k–ε turbulence model with enhanced wall treatment. *Beni-Suef University Journal of Basic and Applied Sciences, 3(4),* 269–277.
39. Zhang, S., Yao, Z., Wu, H., Zhong, Q., Tao, R. et al. (2022). A new turbulent viscosity correction model with URANS solver for unsteady turbulent cavitation flow computations. *Journal of Fluids Engineering, 144(9),* 091403.
40. Chen, W., Luo, Z., Li, X., Lu, S., Guo, F. (2023). Numerical study of temperature separation characteristics of vortex tubes: Effects of structural parameters and modeling of cooling performance correlations. *Thermal Science and Engineering Progress, 39,* 101715.
41. Habchi, C., Oneissi, M., Russeil, S., Bougeard, D., Lemenand, T. (2021). Comparison of eddy viscosity turbulence models and stereoscopic PIV measurements for a flow past rectangular-winglet pair vortex generator. *Chemical Engineering and Processing-Process Intensification, 169,* 108637.
42. Xie, S. F., Wang, Y., Liu, Z. C., Zhu, Z. T., Ning, C. et al. (2015). Optimization of centrifugal pump cavitation performance based on CFD. *IOP Conference Series: Materials Science and Engineering, 72,* 032023.
43. Ahn, S. H., Xiao, Y., Wang, Z., Luo, Y., Fan, H. (2018). Unsteady prediction of cavitating flow around a three dimensional hydrofoil by using a modified RNG k-ε model. *Ocean Engineering, 158,* 275–285.
44. You, Y., Seibold, F., Wang, S., Weigand, B., Gross, U. (2020). URANS of turbulent flow and heat transfer in divergent swirl tubes using the k-ω SST turbulence model with curvature correction. *International Journal of Heat and Mass Transfer, 159,* 120088.
45. Menter, F. R. (1994). Two-equation eddy-viscosity turbulence models for engineering applications. *AIAA Journal, 32(8),* 1598–1605.
46. Menter, F. (1993). Zonal two equation kw turbulence models for aerodynamic flows. *23rd Fluid Dynamics, Plasmadynamics, and Lasers Conference*. Orlando, Florida, USA.
47. Singhal, A. K., Athavale, M. M., Li, H., Jiang, Y. (2002). Mathematical basis and validation of the full cavitation model. *Journal of Fluids Engineering, 124(3),* 617–624.
48. Franc, J. P. (2007). The Rayleigh-Plesset equation: A simple and powerful tool to understand various aspects of cavitation. *Fluid Dynamics of Cavitation and Cavitating Turbopumps, 496,* 1–41.
49. Shah, Y. G., Vacca, A., Dabiri, S. (2018). Air release and cavitation modeling with a lumped parameter approach based on the Rayleigh-Plesset equation: The case of an external gear pump. *Energies, 11(12),* 3472.
50. Rong, G., Cheng, M., Sheng, Z., Liu, X., Zhang, Y. et al. (2022). Investigation of counter-rotating shock wave and wave direction control of hollow rotating detonation engine with Laval nozzle. *Physics of Fluids, 34(5),* 056104.
51. Zhang, R., Cong, T., Tian, W., Qiu, S., Su, G. (2015). Prediction of CHF in vertical heated tubes based on CFD methodology. *Progress in Nuclear Energy, 78,* 196–200.
52. Lu, H., Zhao, W. (2019). CFD prediction of dust pollution and impact on an isolated ground-mounted solar photovoltaic system. *Renewable Energy, 131,* 829–840.
53. Murali-Girija, M., Koukouvinis, F., Karathanassis, I. K., Gavaises, M. (2019). Numerical simulation of three-phase flow in an external gear pump using immersed boundary approach. *Applied Mathematical Modelling, 72,* 682–699.
54. Yoon, Y., Park, B. H., Shim, J., Han, Y. O., Hong, B. J. et al. (2017). Numerical simulation of three-dimensional external gear pump using immersed solid method. *Applied Thermal Engineering, 118,* 539–550.

55. McNulty, P. J., Pearsall, I. S. (1982). Cavitation inception in pumps. *Journal of Fluids Engineering, 104,* 99–104.

56. Jing, T., Cheng, Y., Wang, F., Bao, W., Zhou, L. (2020). Numerical investigation of centrifugal blood pump cavitation characteristics with variable speed. *Processes, 8(3),* 293.

57. Lin, Z., Ruan, X., Zou, J., Fu, X. (2014). Experimental study of cavitation phenomenon in a centrifugal blood pump induced by the failure of inlet cannula. *Chinese Journal of Mechanical Engineering, 27(1),* 165–170.

58. Zhang, B., Zhao, C., Hong, H., Cheng, G., Yang, H. et al. (2022). Optimization of the outlet unloading structure to prevent gaseous cavitation in a high-pressure axial piston pump. *Proceedings of the Institution of Mechanical Engineers, Part C: Journal of Mechanical Engineering Science, 236(7),* 3459–3473.

59. Peng, H., Zhang, P. (2018). Numerical simulation of high speed rotating waterjet flow field in a semi enclosed vacuum chamber. *Computer Modeling in Engineering Sciences, 114(1),* 59–73. https://doi.org/10.3970/cmes.2018.114.059

60. Alsedrani, M. Q., Chala, G. T. (2023). Investigation of the effects of silica nanofluid for enhanced oil recovery applications: CFD simulation study. *Arabian Journal for Science and Engineering, 48(7),* 9139–9158.

61. Yin, F. L., Nie, S. L., Xiao, S. H., Hou, W. (2016). Numerical and experimental study of cavitation performance in sea water hydraulic axial piston pump. *Proceedings of the Institution of Mechanical Engineers, Part I: Journal of Systems and Control Engineering, 230(8),* 716–735.